Supplemental Data

Stepping, Strain Gating, and an Unexpected Force-Velocity Curve for Multiple-Motor-Based Transport

Ambarish Kunwar, Michael Vershinin, Jing Xu, and Steven P. Gross

Supplemental Experimental Procedures

Theoretical model for single Kinesin:

The mechanoenzyme Kinesin moves processively toward the plus end of a microtubule by taking 8-nm steps. The dependence of the velocity V on ATP is successfully reproduced by Michaelis-Menten kinetics that describe binding of a kinesin head, denoted by K, to an ATP molecule and the subsequent hydrolysis according to:

$$K + \mathrm{ATP} \underset{k_{\mathrm{off}}}{\overset{k_{\mathrm{on}}}{\rightleftharpoons}} K\mathrm{ATP} \xrightarrow{k_{\mathrm{cat}}} K + \mathrm{ADP} + \mathrm{P_i}. \tag{1}$$

, where k_{on} (k_{off}) are rate constants for binding (unbinding) of an ATP by the kinesin head, k_{cat} is the rate constant of catalysis or hydrolysis of ATP, and Pi is the phosphate ion which is released upon hydrolysis. In the above expression reversal of ATP hydrolysis has been ignored since its contribution is very small [1]. This leads to the Michaelis-Menten expression for the velocity V of the motor moving along the microtubule

$$V = \frac{V_{\max}[ATP]}{[ATP] + K_m}, \tag{2}$$

where V_{max} is the maximum kinesin velocity at saturating ATP, and is given by the expression

$$V_{max} = k_{\mathrm{cat}} d\varepsilon(F) . \tag{2.1}$$

Here, d = 8 nm is the step size, F is the load, and [ATP] is the ATP concentration. $\varepsilon(F)$ is the load-dependent coupling efficiency between ATP hydrolysis and mechanical stepping. It is independent of ATP concentration. In order to interpolate between 100% efficiency at no load and zero efficiency at the stalling force F_o , the following form for $\varepsilon(F)$ has been chosen[3]:

$$\varepsilon(F) = 1-(F/F_o)^2 . \tag{2.2}$$

Above, K_m is the Michaelis-Menten constant, given by the expression

$$K_m = (k_{cat} + k_{off})/k_{on} . \tag{2.3}$$

The enzymatic properties of molecular motors are affected by any applied load. This load dependence is modeled by including it in the rate constants. Kinesin experiments indicate that increasing load results in a decrease in $V_{\max}$ and an increase in K_{m}. The decrease in V_{max} is accounted for by the coupling efficiency, which allows k_{cat} to be taken to be load independent. To account for the observed increase in K_m, either k_{on} should decrease or k_{off} should increase (or both) with increasing load. Here it was assumed that k_{off} increases with increasing load, following [3]:

$$k_{\mathrm{off}} = k_{0\ \mathrm{off}} \exp[F\mathrm{d_l}/k_B T], \qquad (2.4)$$

where k_B is the Boltzmann's constant, T = 300 K is the temperature in Kelvin, $k_{0\ \mathrm{off}}$ = 55 sec^{-1}, and $\mathrm{d_l}$=1.6 nm.

A Monte-Carlo implementation of the above model correctly reproduces the experimentally known dependence of velocity on applied load and ATP concentration [3] however it doesn't model the dependence of run length on applied load and ATP concentration. To develop a complete Monte-Carlo description, which also captures the experimentally known processivity of Kinesin, we make use of the model for Kinesin described in [2]. According to this model, Kinesin can detach from the microtubule from two different states, which occur before and after ATP binding. The probability of detachment from the state before ATP binding is given by $P_1=B/[ATP]$ per cycle, where B is a constant. The probability of detachment from the state after ATP binding is given by $P_2= (1/A)exp(F\delta_l/k_BT)$, where A is the maximum number of steps that kinesin takes under zero load before detaching from microtubule. Therefore, the probabilities of detachments from these two different routes (per unit time) are given by the expressions:

$$P_{\mathrm{det}\,ach1} = P_1.P_{step} = \frac{B.P_{step}}{[ATP]} \qquad (3)$$

$$P_{\mathrm{det}\,ach2} = P_2.P_{step} = \frac{e^{F\delta_l/k_BT}.P_{step}}{A} \qquad (4)$$

where

$$P_{step} = \frac{k_{cat}.\varepsilon(F)[ATP]}{[ATP]+K_m} \qquad (5)$$

The proccessivity L reflecting the two different routes for dissociation of Kinesin from the Microtubule is given by the following expression [2]

$$L = \frac{d.[ATP].Ae^{-F\delta_l/k_BT}}{[ATP]+B(1+Ae^{-F\delta_l/k_BT})} \quad . \qquad (6)$$

Equations (2) and (6) give a very good fit to the known experimental data [2] for the following parameters: k_{on} = 2 × 10^6 M^{-1}•sec^{-1}, and k_{cat} = 105 sec^{-1} , $K_{0\ off}$=55 sec^{-1}, B=0.029 μM, A=107, d_l=1.6nm, δ_l=1.3nm and F_o = 8 pN. Unless explicitly stated otherwise, simulations were done at saturating ATP, i.e. [ATP]=3mM.

Monte-Carlo algorithm for single Kinesin:

We describe the states of single Kinesin on the microtubule by a two-state variable s (where s is 0 or 1): s=0 represents the state without an ATP molecule, and s=1 represents a state with kinesin bound to an ATP molecule. The procedure updates the state of the motor(s) for all times t between 0 and t_{max} in increments of Δt. Note that here the time step Δt is chosen in such a way that it is sufficiently smaller than the typical time scale over which the fastest process in the mechano-chemical cycle occurs. The update procedure for each configuration is described below.

A. Initial condition: t=0, s=0, x=0, where x is the position of the motor on the microtubule.

B. Updating procedure: Repeat the following steps up to t_{max} in increments of Δt.

(i) if $t > t_{max}$ goto step C
(ii) Detachment of Kinesin: calculate $P_{detach1}$ and $P_{detach2}$. First try detachment with probability $P_{detach1}$. If detachment occurs, goto step C, else try detachment with probability $P_{detach2}$. If detachment occurs goto step C else goto step (iii)
(iii) Binding/Unbinding of ATP: Switch the value of s with probability $P_{on} = k_{on}[ATP]\Delta t$ or $P_{off} = k_{off}\Delta t$, depending on whether the current value of s is 0 or 1 respectively. At saturating ATP levels and moderate loads, the binding of ATP is the fastest process. At saturating ATP (say 3mM) ATP binding would take typically 10^{-4} s provided $k_{on}=2\times10^{6}$ $M^{-1}.S^{-1}$. Therefore we choose $\Delta t=10^{-5}$ s [3].
(iv) Hydrolysis and stepping: If s=1 after step (iii), hydrolysis occurs with probability $P_{cat} = k_{cat}\Delta t$. After hydrolysis, s=0 and x is changed to x+d with probability $\varepsilon(F)$

C. Calculation of Run length and Velocity:
Run length is the current value of x. Velocity is obtained dividing current position x by the current time t.

The results obtained from this improved Monte-Carlo algorithm have been plotted in Supplement Fig. S1 and Supplement Fig. S2, along with the original theoretical description provided in [2] that matches the single-molecule experiments in [2] quite well for the following parameters: k_{on} = 2×10^{6} $M^{-1}\bullet sec^{-1}$, and k_{cat} = 105 sec^{-1} , $K_{0\,off}$=55 sec^{-1}, B=0.029 μM, A=107, d_l=1.6nm, δ_l=1.3nm and F_o = 8 pN, as described earlier in this supplement. As expected, our Monte-Carlo Simulations reproduce the original theory quite well.

Rescaling of single motor model for different stall forces Our simulated motor reproduces reported [2] single-molecule behavior for F_0=8 pN. However, frequently, observed experimental stall forces are different. To rescale our model for different values of stalling force F_0 we use following form of probability P_2 (see equation 4)

$$P_2 = (1/A)\exp((8/F_0)(F\delta_l/k_BT))$$

This new form of probability P_2 reduces the runlength of a single motor by ~70% at half of the stalling force for any F_0.

Monte Carlo Algorithm for the multiple motor model:

A detailed description of the sequence of events in the multi-motor Monte-Carlo simulation is provided below; however the basic sequence of events is as follows. For each time step, we visit each of the N motors and determine their tentative states (attached or detached) and positions. To calculate the tentative state and position of a motor which is currently unattached, we allow it to attach with a probability determined by the assumed 'on-rate' within a region which can be explored by the unattached motor. To determine the tentative state and position of a motor which is currently attached, we explore all the three possibilities: it can remain stationary, advance, or detach. To determine what the motor does, we first calculate the force it experiences. Force felt by a given motor depends on the position relative to the position of the bead. The method of calculation of bead position in Model A and model B is explained below. Once the bead position is calculated, we know the force the motor in question is experiencing. We then determine if it steps, remains stationary, or detaches, where the probability of each event is determined from the single-kinesin model. Once we have determined the tentative states and positions of all N motors, we update the states and positions of all motors simultaneously. We calculate the new position of the bead using the new states and positions and time step is finished. We then record the number of motors engaged, their locations, and the overall location of the cargo.

We put a number of motors, N, on the cargo, where the motor heads are attached to the cargo via a linkage (stalk) of length l. In this case, l is an idealized motor with a natural length of 110 nm, and exerts a restoring force only when it is stretched beyond the natural length. It has no compressional rigidity, i.e. it buckles without resistance when compressed. These linkages are localized at a single spot on the cargo. Motors bound to a microtubule walk on a lattice, where each binding site of the motors heads are 8 nm apart. The update procedure for each configuration of our multiple motor model is described below:

Initial condition: We denote the current position of the cargo by x, and current time by t, and the number of *engaged* motors by e (motors whose heads are actually bound to microtubule). Let us assume we want to start with the initial condition where only n motors are initially attached to the microtubule out of total N number of motors on the cargo. We hold the cargo's center of mass at position $x=x_{hold}$ above the microtubule lattice and allow a number of motors n to attach to the microtubule. The motors are allowed to attach to any binding site on the microtubule which is within distance l on either side of the cargo. Once motors are attached to the microtubule we calculate the initial position of the cargo's center of mass x_{start} which depends on the position of the motors heads, length of linkage, stiffness of linkage and applied load F (described later in this section). Thus at $t=0$, $x=x_{start}$ and $e=n$.

Updating procedure: We update the state of the model in steps of Δt, up to time $t_{max,}$ where the basic time step Δt is identical to that used in the single molecule model. At any time step t, the update procedure consists of following steps:

i) If $t > t_{max}$, goto step (vi)
ii) *Determine the tentative states and tentative positions of the motors:* We determine the tentative states and tentative positions of all the N motors in the following way.

If a motor is in a detached state, then motor doesn't feel any load. However if the motor is attached to the microtubule, forward or backward load F_i felt by the i^{th} motor is obtained by multiplying the extension of its linkage Δl_i by the linkage stiffness k. We describe the nucleotide-states of motor by a two-state variable s_i (where s_i is 0 or 1). s_i =0 represents the state of i^{th} motor without an ATP molecule at time step t, and s_i=1 represents i^{th} motor binding an ATP molecule (i=1, 2,…N). In the following paragraph $x_i(t)$ denotes the state of the i^{th} motor at time t and $x_i(t,Tmp)$ denotes the calculated tentative position of the i^{th} motor at time t, i.e. the position at which the i^{th} motor would be at time step t+1. Similarly, $S_i(t)$ denotes the state (attached/detached) of the i^{th} motor at time t, and $S_i(t,Tmp)$ denotes the calculated tentative state of the i^{th} motor at time t, i.e. the state in which the i^{th} motor would be at time step t+1. Here, $S_i(t)$=0 signifies that the i^{th} motor is in detached state at time t, and $S_i(t)$=1 signifies that the i^{th} motor is in attached state at time t.

Tentative states and tentative positions of the detached and attached motors are determined according to following rules.

A1. Determining the tentative state and tentative position of a detached motor: if the selected motor is in a detached state, it gets an opportunity to (re)attach to the microtubule. The motor is allowed to attach to any binding site on the microtubule, with probability P_a, which is within distance l on either side from the center of mass of the cargo. If it does set $S_i(t,Tmp)$=1 and go to the next motor (if any).
A2. Determining the tentative state and tentative position of a attached motor: tentative states and tentative positions of attached motors are calculated in the following steps (B1 to B7)

B1. calculatation of k_{off}: k_{off} is calculated using equation (2.4) provided the load felt by motor is in a backward direction. For forward load we use F_i=0 in equation (2.4) because a forward load does not alter the kinetic cycle of kinesin and therefore the motor moves as if it was moving under zero load [4].

B2. Calculation of P_2: P_2 is calculated using the expression $(1/A)exp(F_i\delta_i/k_BT)$ irrespective of the direction of the load (i.e. forward or backward) on the motor. We assume that a forward or backward load would have similar effect on detachment kinetics.

B3. Calculation of $\varepsilon(F_i)$: $\varepsilon(F_i)$ is calculated using equation (2.2) for backward loads $F_i \leq F_0$. For backward load greater than F_0 (i.e. load greater than stall) $\varepsilon(F_i)$ =0. Again, a forward load does not alter the kinetic cycle of kinesin and therefore the motor moves as if it was moving under zero load; therefore we put F_i=0 for forward loads in equation(2.2)

B4. P_{step} is calculated using values of k_{off} and $\varepsilon(F_i)$ in equation (2.3) and (5).

B5. Detachment kinetics: calculate $P_{detach1}$ and $P_{detach2}$ using equation (3) and (4). First try detachment with probability $P_{detach1}$. If detachment occurs then set s_i=0, $S_i(t,Tmp)$=0 and go to next motor (if any), else try detachment with probability $P_{detach2}$. If detachment occurs set s_i=0, $S_i(t,Tmp)$=0 and go to next motor (if any), else goto step (B6).

B6. Binding/Unbinding of ATP: switch the value of s_i with probability $P_{on} = k_{on}[ATP]\Delta t$ or $P_{off} = k_{off}\Delta t$, depending on whether the current value of s_i is 0 or 1 respectively.

B7. Hydrolysis and stepping: If s_i=1, after step (B6), hydrolysis occurs with probability $P_{cat} = k_{cat}\Delta t$. After hydrolysis s_i=0 and and $x_i(t,Tmp)$ is set to $x_i(t)$+d with probability $\varepsilon(F_i)$. If motor

does not hydrolyze ATP or fails to step with probability $\varepsilon(F_i)$, after ATP hydrolysis then we check whether $F_i \geq F_0$. If $F_i \geq F_0$, then we implement the detachment kinetics of kinesin under super stall conditions by allowing the motor to detach with probability P_{back}. We choose $P_{back}=2\ s^{-1}$, which was previously experimentally determined for kinesin [5]. If detachment occurs, then set $s_i=0$, $S_i(t,Tmp)=0$ and go to next motor (if any). We again take the detachment kinetics under super stall to be independent of the direction of the load.

iii) *Updating states and tentative positions of the motors:* Once we have calculated the tentative state $S_i(t,Tmp)$ and tentative position $x_i(t,Tmp)$ for all N motors, we update the states and positions of all the N motors simultaneously. To do this, We set $S_i(t+\Delta t)= S_i(t,Tmp)$ and $x_i(t+\Delta t)= x_i(t,Tmp)$ for all i (i=1, 2,…N).

(iv) Calculating number of engaged motors: calculate e, If e=0 then record the final position of the cargo $x_{final}=x$, and go to step (vi), else go to step (v).

(v) Updating position of the cargo: the method for calculating the position of the center of mass of the cargo x after updating the motor is outlined below for Model A and Model B.

Model A: In model A, the position of the bead is determined by balancing the externally applied force F (if any) with the force that each of the bound motors supports. To do this, first find out the position of the two outermost motor heads, say x_{max} and x_{min}. (For a cargo driven by single motor $x_{max}=x_{min}$). Check if the cargo is loaded or unloaded (i.e. F=0 or F≠0). If the cargo is unloaded go to (A), else go to (B).

A. Unloaded cargo (*F=0*): if $x_{max}-x_{min} \leq 2l$ (where l is the natural length of linkage) this would mean that none of the linkages are stretched. In this case the position of the center of mass of the cargo is given by $x=(x_{max}+x_{min})/2$, which essentially captures the fact that for a cargo driven by a single motor, when unloaded, the center of mass of the cargo on the average is likely to be found at the position of motor head, and for a cargo driven by multiple motors, when it is unloaded and linkages are not stretched, the center of mass of the cargo on the average will be found between the two outermost motor heads.
If $x_{max}-x_{min} > 2l$ then some of the linkages are stretched; go to B1

B. Loaded cargo (*F≠0*): Any non-zero load is supported by the motor(s), which causes the linkages to stretch.
B1. Calculate the new extension of the linkage for each motor, using the current bead position and the new position of the motor after stepping.
B2. Calculate the equilibrium extension of each linkage. The equilibrium extension of each motor linkage is obtained by requiring that the net force on the cargo is zero. Use the equilibrium extension of any linkage to calculate the new position of the center of mass of the cargo.

Model B: In model B, the position of the bead is determined by an externally applied load (if any), as well as thermal noise. In the absence of any force, the bead would execute a Brownian motion due to the thermal noise. Over a time interval of Δt, the displacement of the bead due to these thermal kicks can be drawn from a normal distribution with a mean-square displacement $2D\Delta t$, where D is the diffusion constant of the bead. The diffusion constant D is related to the friction constant ξ by the Einstein relation $\xi=k_BT/D$, reflecting the influence of viscous drag on the bead's motion. We neglected the thermal motion of the springs; our simulation is dominated by the thermal motion of the bead. Our springs are "special springs" in that

they exert a restoring force only when they are stretched. For the bead, the friction constant ξ is related to viscosity of the medium η and radius r of the bead by the relation

$$\xi=6\pi\eta r.$$

If the bead were subject to a net force f then this would cause the bead to move with velocity $v_{drift}=(f/\xi)$. To calculate the net motion of the bead over time interval Δt we superimpose the deterministic drift $x_{drift}=v_{drift}.\Delta t=(f/\xi)\Delta t$ on the random displacements x_{random} where the displacements are drawn from a normal distribution with mean square displacement $2D\Delta t$ [6]. To summarize, the bead displacement at time t and $t+\Delta t$ are related by:

$$\vec{x}(t+\Delta t)=\vec{x}(t)+\vec{x}_{random}+\vec{x}_{drift}=\vec{x}_t+\vec{x}_{random}+\frac{\vec{f}}{\xi}\Delta t$$

The net force f on the bead is given by

$$\vec{f}=\vec{F}+\sum_{i=1}^{N}\vec{f}_i$$

where f_i is the restoring force exerted by i^{th} motor on the bead, whose magnitude depends on the extension of i^{th} linkage, and is given by $k.\Delta l_i$.

vi) Calculation of travel distance: x_{final} is the current value of x. The travel distance of the cargo is given by $x_{final}-x_{start.}$
In model B, any non-zero external force initially can cause the bead to drift in the direction of the force. Therefore, in order to measure the travel distance correctly we set x_{start} after 0.2 milliseconds in Model B instead of at t=0.

Average velocities and average walking distance (persistence) in steady-state model:

In the steady-state model [7], the average velocity of a cargo is given by

$$v_{eff}=\sum_{n=1}^{N}v_n\frac{P_n}{1-P_0} \qquad (7)$$

Where P_n denotes the probability that the cargo is bound to the microtubule by n motors and v_n is is the corresponding velocity. P_n is given by expression:

$$P_n=P_0\prod_{i=0}^{n-1}\frac{\pi_i}{\varepsilon_{i+1}} \qquad \text{where} \quad P_0=\left[1+\sum_{n=0}^{N-1}\prod_{i=0}^{n}\frac{\pi_i}{\varepsilon_{i+1}}\right]^{-1} \qquad (8)$$

Above, N denotes the total number of motors bound to the cargo, π_n is the motor (re)attachment rate or 'on rate' when n motors are bound to microtubule and ε_n is the detachment rate or 'off rate' when n motors are bound to the microtubule.

The average walking distance or persistence is given by the expression [7]

$$< x_b >= \frac{v_1}{\varepsilon_1}\left[1+\sum_{n=0}^{N-1}\prod_{i=0}^{n}\frac{v_{i+1}\pi_i}{v_i\varepsilon_{i+1}}\right] \quad (9)$$

v_n, ε_n and π_n are related to the single motor velocity v, 'off rate' ε and 'on rate' π_{ad} by the expressions:

$$v_n = v\left(1-\frac{F}{nF_s}\right) \quad (10)$$

$$\varepsilon_n = n\varepsilon \exp\left(\frac{F}{nF_d}\right) \quad (11)$$

$$\pi_n = (N-n)\pi_{ad} \quad (12)$$

Here F_s is the stalling force of a single motor, F_d is the detachment force for a single motor, and F is externally applied load. Further details of the steady-state model (equations (8)-(12)) can be found in [7].

Additional data for many figures discussed in the main text:

Figure 2:

Fig. 2A) The data for stepsize distribution was obtained from 50 configurations, each running for a maximum time of 100 sec (1 time step=10^{-5} sec), where each configuration was started with the initial condition that both motors are attached to the microtubule. Simulation for each configuration was stopped when either all motors had detached from microtubule, or 100 seconds had passed. Applied load =3 pN

Fig 2B) The data for stepsize distribution was obtained from 20 configurations, each running for a maximum of 100 sec (1 time step=10^{-5} sec), where each configuration was started with the initial condition that both motors are attached to the microtubule. Simulation for each configuration was stopped when either all motors had detached from microtubule or 100 seconds had passed. For 10 configurations, the bead was moving under an external load of 3pN, and for another 10 configurations the bead was moving under an external load of 4pN (this was done to match experimental conditions).

Fig 2C) The data was obtained from 10 configuration, where each configuration was running for 100 sec. Simulation for each configuration was stopped when all motors had detached. External load force=0 pN.

Fig 2D) The data was obtained from 10 configuration, where each configuration was running for a maximum time of 100 sec. Simulation for each configuration was started with the initial condition that both motor are attached randomly to the microtubule, and

simulation was stopped when all motors had detached. External load force=0 pN.

Figure 3:
Fig 3C. Original 'in silico' data was generated for 5000 configurations, where each configuration ran for a maximum time of 100 sec. Simulation for each configuration was started with the initial condition that both motor were attached randomly to the microtubule and simulation was stopped when all motors had detached. (On rate for each motor was $5s^{-1}$ and trap stiffness was 0.09205 pN/nm)

Figure 4:
Fig4 A B. As already indicated in the main text, the initial and final conditions are same as Fig 5. The average velocity was calculated using the velocities calculated over a time window of 0.5 sec in the steady state. However for the single motors, the average velocity was calculated over the entire run-length.

Figure 5:
Fig 5A. Monte Carlo results were obtained by averaging over 1000 samples, each having a duration of 100 s (1time step=10^{-5}s). Simulation was started with the initial condition that all motors were randomly attached to the microtubule, and simulation was stopped if all motors had detached.

Fig 5B. Same as Fig 5A; Monte Carlo results were obtained by average over 1000 samples each having a duration of 100 s (1time step=10^{-5}s). Simulation was started with the initial condition that all motors are randomly attached to the microtubule and simulation was stopped if all motors had detached.

Fig 5C. Same as Fig 5A; Monte Carlo results were obtained by average over 1000 samples each having a duration of 100 s (1time step=10^{-5}s). Simulation was started with the initial condition that all motors are randomly attached to the microtubule and simulation was stopped if all motors had detached.

Fig 5D. Same as Fig 5A; Monte Carlo results were obtained by average over 1000 samples each having a duration of 100 s (1time step=10^{-5}s). Simulation was started with the initial condition that all motors are randomly attached to the microtubule and simulation was stopped if all motors had detached.

Figure 6:
Fig 6 A. There is no averaging here. In this case a random configuration was chosen for each configuration. A configuration which had a long runtime was selected in each case, so that we could show that strain-gating sequence for a longer duration.

Fig 6B. Monte Carlo results were obtained by average over 1000 samples each having a duration of 100 s (1time step=10^{-5}s). Initial and final condition same as Fig 6A.

Fig 6C. Data for the force distribution was obtained from 1000 samples each having a duration of 100 s (1time step=10^{-5}s). Simulation was started with the initial condition that all motors are randomly attached to the microtubule and simulation was stopped if all motors had detached.

Figure 7:
Fig 7A. Monte Carlo results were obtained by average over 1000 samples each having a duration of 100 s (1time step=10^{-5}s). Simulation was started with the initial condition that all motors are randomly attached to the microtubule and simulation was stopped if all motors had detached. Average velocity was calculated in the same way as in Fig 4.
Fig 7B Same as Fig 7A

On the term 'strain gating', and past studies investigating motor-motor coupling:

There has been significant work (see e.g. [8]) investigating how the enzymatic cycles of two heads of a dimeric motor such as kinesin are coordinated, so that they remain 'out of sync', in order to allow the motor to walk processively down a filament, undergoing multiple enzymatic cycles while having one head always bound to the filament. It seems clear that this is maintained through some form of 'strain-gating', where the internally generated load due to spatial separations between the two heads leads to appropriately staggered enzymatic cycles. This *internally generated* strain, controlling enzymatic cycles, is different from our *externally generated* load (due to a load applied to the cargo), yet it has a very similar effect, making the motors go through their enzymatic cycles at defined times with respect to each other. Other work by Diehl et al[9] investigated a situation very similar to the case of Guydosh and Block, because they investigated the role of linkage stiffness in allowing monomeric heads that were otherwise unprocessive to work together.

A possible relationship to the "catch-bond" behavior reported by Guo and Guilford (PNAS, 2006):

A reviewer of the manuscript pointed out an intriguing relationship between our findings and the acto-myosin system. Guo and Guilford [10] report that the life time of the actomyosin bond first increases with increasing load, and then decreases with increasing load after reaching a maximum at ~6 pN. There is likely some similarity between this catch bond behavior and kinesin' average life time on microtubule. We notice (Supplement, Fig S3) that the average binding time of kinesin on the microtubule starts increasing on applying load greater than ~3 pN up to stall force (6 pN) and then it drops to 0.5 seconds after reaching stall force. The slight increase in processivity that we

predict (around single motor stall, Fig 5D, main text) is due to this increased average binding time of the motor supporting a moderately high load. One would see this effect for very stiff linkage. At very high load, or for a very weak linkage, the backward motions contribute significantly to the overall run-length and obscure the effect. Hence it is only observed at moderate loads.

Supplemental References:

1. Hackney, D.D. (1996). The kinetic cycles of myosin, kinesin, and dynein. Annu Rev Physiol *58*, 731-750.
2. Schnitzer, M.J., Visscher, K., and Block, S.M. (2000). Force production by single kinesin motors. Nat Cell Biol *2*, 718-723.
3. Singh, M.P., Mallik, R., Gross, S.P., and Yu, C.C. (2005). Monte Carlo modeling of single-molecule cytoplasmic dynein. Proc Natl Acad Sci U S A *102*, 12059-12064.
4. Block, S.M., Asbury, C.L., Shaevitz, J.W., and Lang, M.J. (2003). Probing the kinesin reaction cycle with a 2D optical force clamp. Proc Natl Acad Sci U S A *100*, 2351-2356.
5. Coppin, C.M., Pierce, D.W., Hsu, L., and Vale, R.D. (1997). The load dependence of kinesin's mechanical cycle. Proc Natl Acad Sci U S A *94*, 8539-8544.
6. Beausang, J.F., Zurla C, Finzi L, Sullivan L, and PC, N. (2007). Elementary Simulation of tethered Brownian motion. . Am. J. Phys. *75*, 520-523.
7. Klumpp, S., and Lipowsky, R. (2005). Cooperative cargo transport by several molecular motors. Proc Natl Acad Sci U S A *102*, 17284-17289.
8. Guydosh, N.R., and Block, S.M. (2006). Backsteps induced by nucleotide analogs suggest the front head of kinesin is gated by strain. Proc Natl Acad Sci U S A *103*, 8054-8059.
9. Diehl, M.R., Zhang, K., Lee, H.J., and Tirrell, D.A. (2006). Engineering cooperativity in biomotor-protein assemblies. Science *311*, 1468-1471.
10. Guo, B., and Guilford, W.H. (2006). Mechanics of actomyosin bonds in different nucleotide states are tuned to muscle contraction. Proc Natl Acad Sci U S A *103*, 9844-9849.

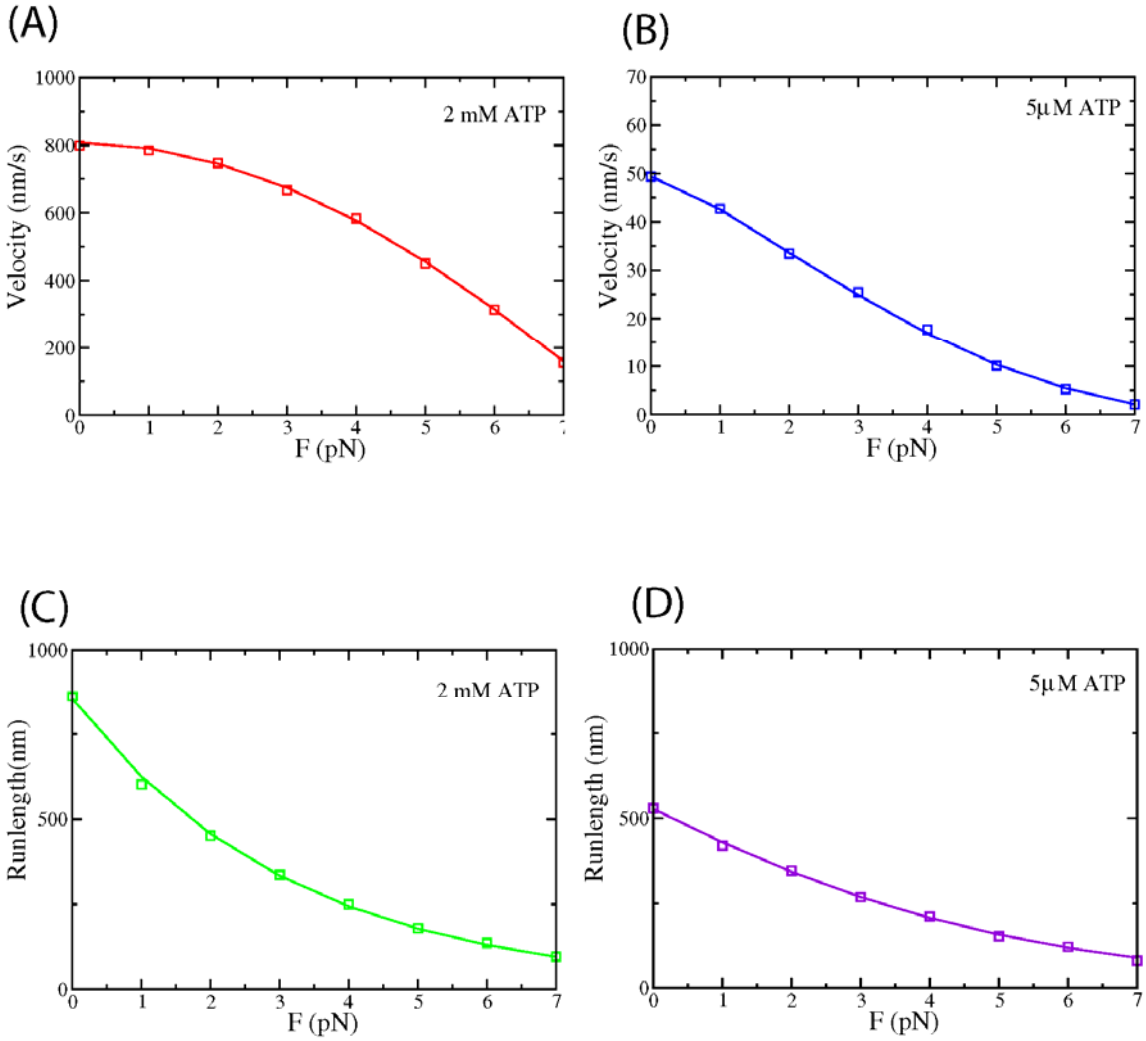

Figure S1. The Monte-Carlo model reproduces known single-molecule kinesin function Dependence of Velocity on load for [ATP]=2 mM **(A)** and [ATP]=5 μM **(B);** dependence of mean travel distance on load for [ATP]=2 mM **(C)** and [ATP]=5 μM **(D).** In each case, the open symbols show the data obtained from Monte-Carlo Simulation. The solid lines in A and B were obtained using equation (2) by choosing the same parameter values as used in simulations and solid line in C and D were obtained using equation (6) by choosing the same parameter values as used in simulations. The parameter values are F_o = 8 pN, k_{on} = 2 × 10^6 M^{-1}•sec^{-1}, and k_{cat} = 105 sec^{-1} , $K_{0\ off}$=55 sec^{-1}, B=0.029 μM, A=107, d_l=1.6nm,δ_l=1.3nm. Note that the solid curves are a good proxy for the single-molecule behavior, because they were previously shown (in [2]) to match single-molecule kinesin experiments extremely well. Monte Carlo results were obtained by averaging over 1000 samples each having a duration of 100 s (1time step=10^{-5}s).

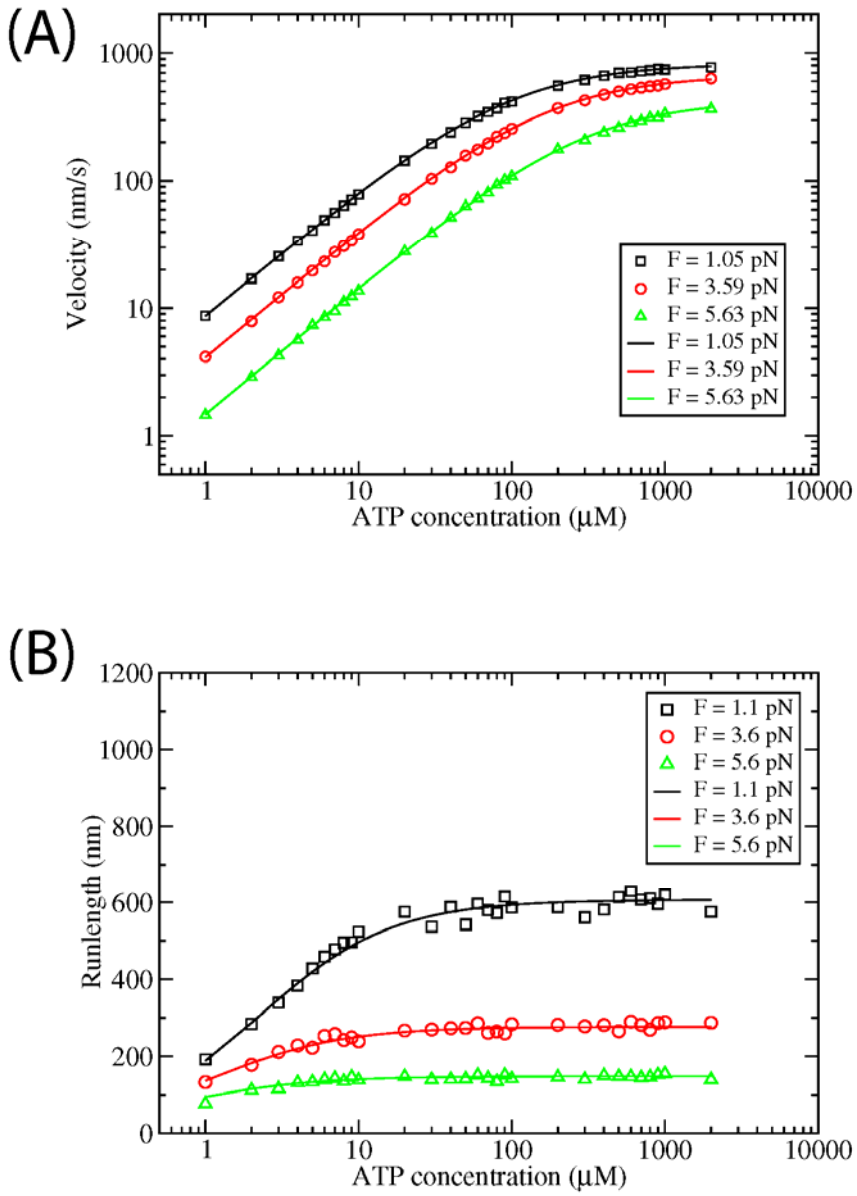

Figure S2. Effect of constant load on single kinesin's mean velocity and travel length, at different ATP concentrations Dependence of Velocity **(A)** and Mean Travel **(B)** on ATP concentration for different loads. Open symbols show the data obtained from Monte-Carlo Simulation. The solid velocity lines (in A) have been obtained by using equation (2) by choosing the same parameter values as used in simulations, while the travel-distance lines (in B) come from equation (6). The parameter values are same as in Supplement Fig. S1. Monte Carlo results were obtained by averaging over 1000 samples each having a duration of 100 s (1time step=10^{-5}s).

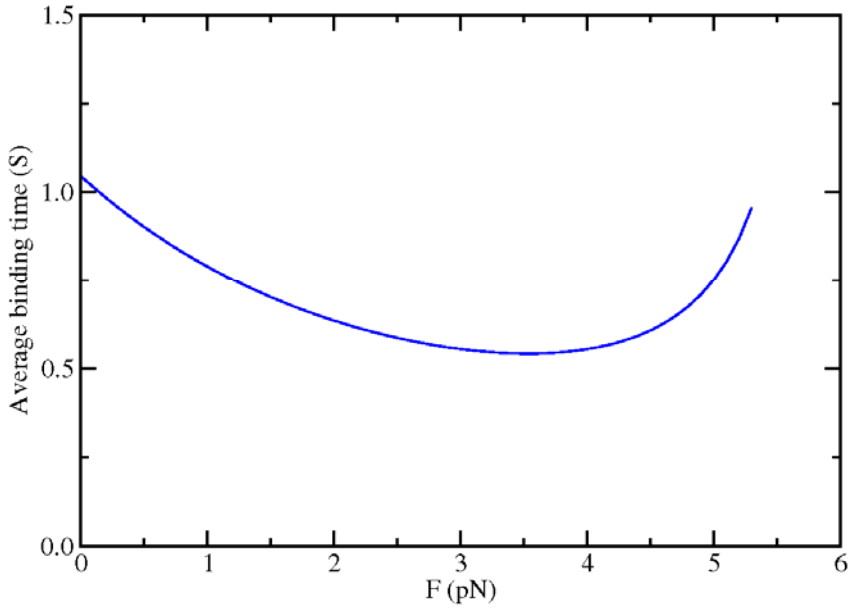

Figure S3. Average time a single kinesin spends attached to the microtubule, as a function of load. This graph results from our simulations using the same parameter values as in Figure 5A (Model A, with a 6 pN stall). Note that essentially the same graph can be obtained entirely from single molecule *in vitro* experimental data, by using the experimentally determined processivity as a function of load (panel b, fig. 3, [2]) and velocity as a function of load (panel b, fig. 2, [2]): for a given force, divide the mean processivity by the mean velocity. This graph is important because it has ramifications for the effect of load on the number of engaged motors, in the multiple-motor case. We note that the applied load affects the average number of engaged motors <n> (<n> ≤ N). A previous steady-state model[7] predicted that <n> decreased monotonically with increasing force, but this is not true in our model. This is because <n> is determined by a competition between each motor's 'on' rate and 'off' rate. The 'on' rate is independent of applied load (the unattached motors feel no load), but as we see in Fig S3, the 'off' rate in time combines effects of load on both velocity (stepping rate) and detachment probability per step (processivity) and is a non-monotonic function of applied load. The number of configurations was the same as Figure 5A, main text.

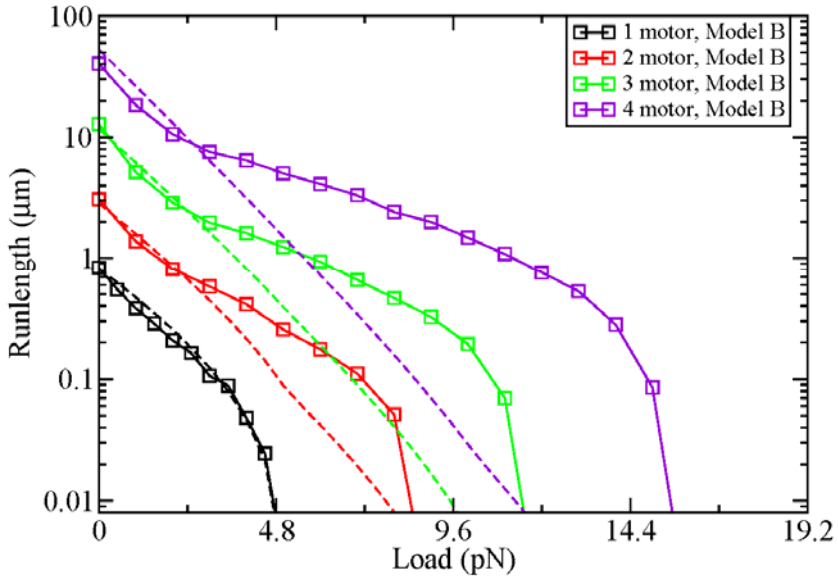

Figure S4. Predicted locations of 2, 3, and 4-motor stalls for Model B and Steady State model when the single-motor stall has been tuned to 4.8 pN. In our model, the one-motor stall is a free parameter, that we tune to match the relevant experimental data. Here, to quantitatively compare stalling force predictions for experiments and theory (see Fig 3, main text), we tuned the single-motor stall to be 4.8 pN. As discussed in the main text, the best way to compare theory and experiment is to simulate cargo motion and analyze the simulated traces in the same way that experiments are analyzed (Fig 3, main text). However, having done that, we note that using the runlength-force curves, we can predict the approximate values of the 2, 3, and 4-motor stalls by determining the location where the mean predicted travel goes to 0.008 μm, i.e. ~ 1 step of the motor. This graph allows comparison of a comparison of the Monte-Carlo Model B and the previously published steady state model with the experiments. The parameter values for Model B are same as Figure 5A andB, except F_o = 4.35 pN. The parameter values for SS model are same as Figure 5 except F_s = 5.1 pN. The number of configurations was the same as Figure 5B, main text.

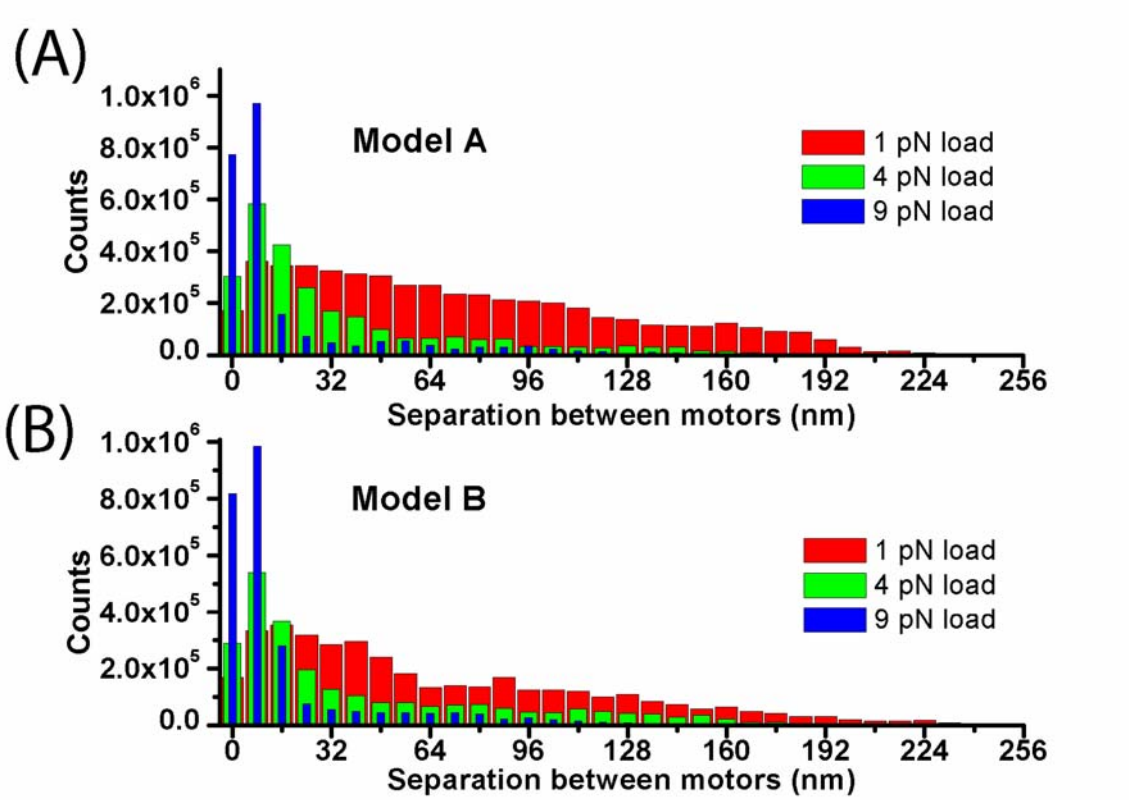

Figure S5. Observation of clustering as a function of load: Distribution of the average separation between the locations that the two motors bind to the microtubule As external load is applied to a cargo moved by two 6 pN-stall kinesin motors , each coupled to the cargo via a 0.32 pN/nm linkage, it is possible that load induces clustering of the motors, where the separation between the locations where the motors attach to the microtubule gets to be quite small. In the simulations, we are able to instantaneously observe the MT-binding locations of each motor, and here summarize the instantaneous difference in the positions of the two. The motors are each 110 nm long (unstretched), so the maximum difference between the two attachment locations is expected to be ~220 nm. We observe very similar behavior for both Model A (A) and Model B (B). For low applied load (1 pN; red bars) we observe no clustering, while there is moderate clustering at intermediate applied load(4pN; green), and strong clustering at high load (9 pN; blue), where the majority of the motors are within 8 nm of each other. Other parameter values are same as in Figure 5. Data was obtained from 100 samples each having a duration of 100 s. Simulation was started with the initial condition that both motors are randomly attached to the microtubule and simulation was stopped when one of the motor detaches.

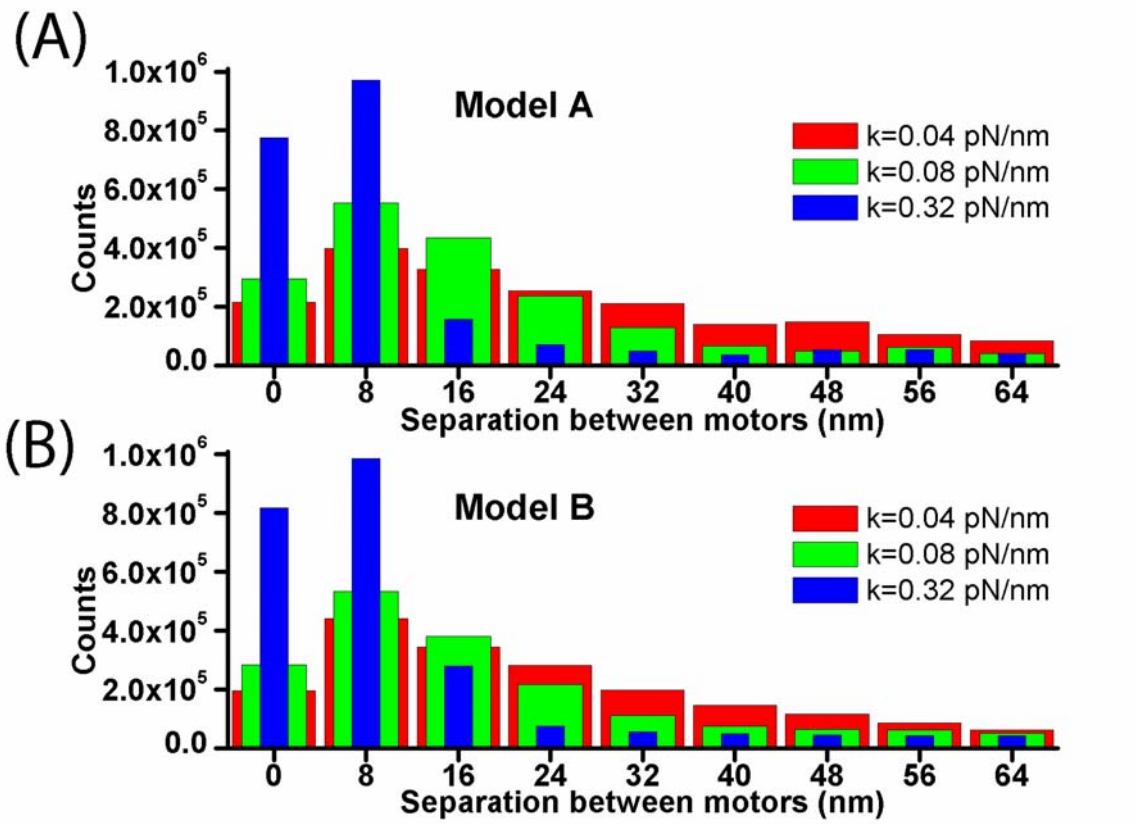

Figure S6. Clustering requires a high-stiffness linkage. As in Fig. S5, we examine the separation between the MT-attachment locations of two motors. Here, the two motors are moving the cargo against 9 pN of externally applied load, but are coupled to the cargo by very weak springs (k=0.04 pN/nm, red bars), weak springs (k=0.08 pN/nm, green bars), or strong springs (k=0.32 pN/nm, blue bars). Strong clustering is observed for the strong springs, but not for the other two cases. Other parameter values are same as in Figure S5. Data was obtained from 100 samples each having a duration of 100 s. Simulation was started with the initial condition that both motors are randomly attached to the microtubule and simulation was stopped when one of the motor detaches.

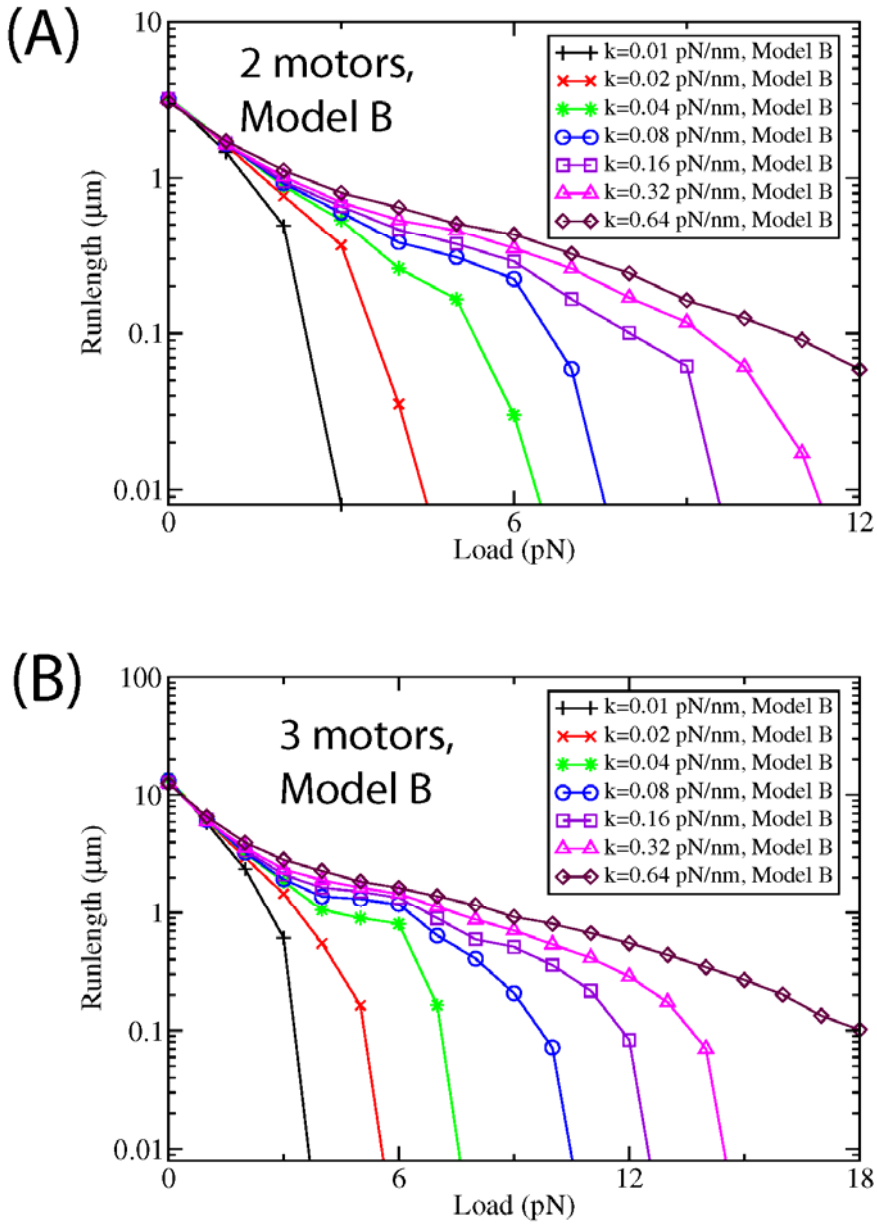

Figure S7. Force-Persistence curves for cargos at different values of linkage stiffness, for 2 **(A)** and 3 **(B)** motors moving according to Model B. These graphs are the companions (and quite similar to) to the graphs reflecting the Model A predictions in the main text (Fig 5C and D). The parameter values are the same as for the Model A. The number of configurations was the same as for Fig 5C, main text.

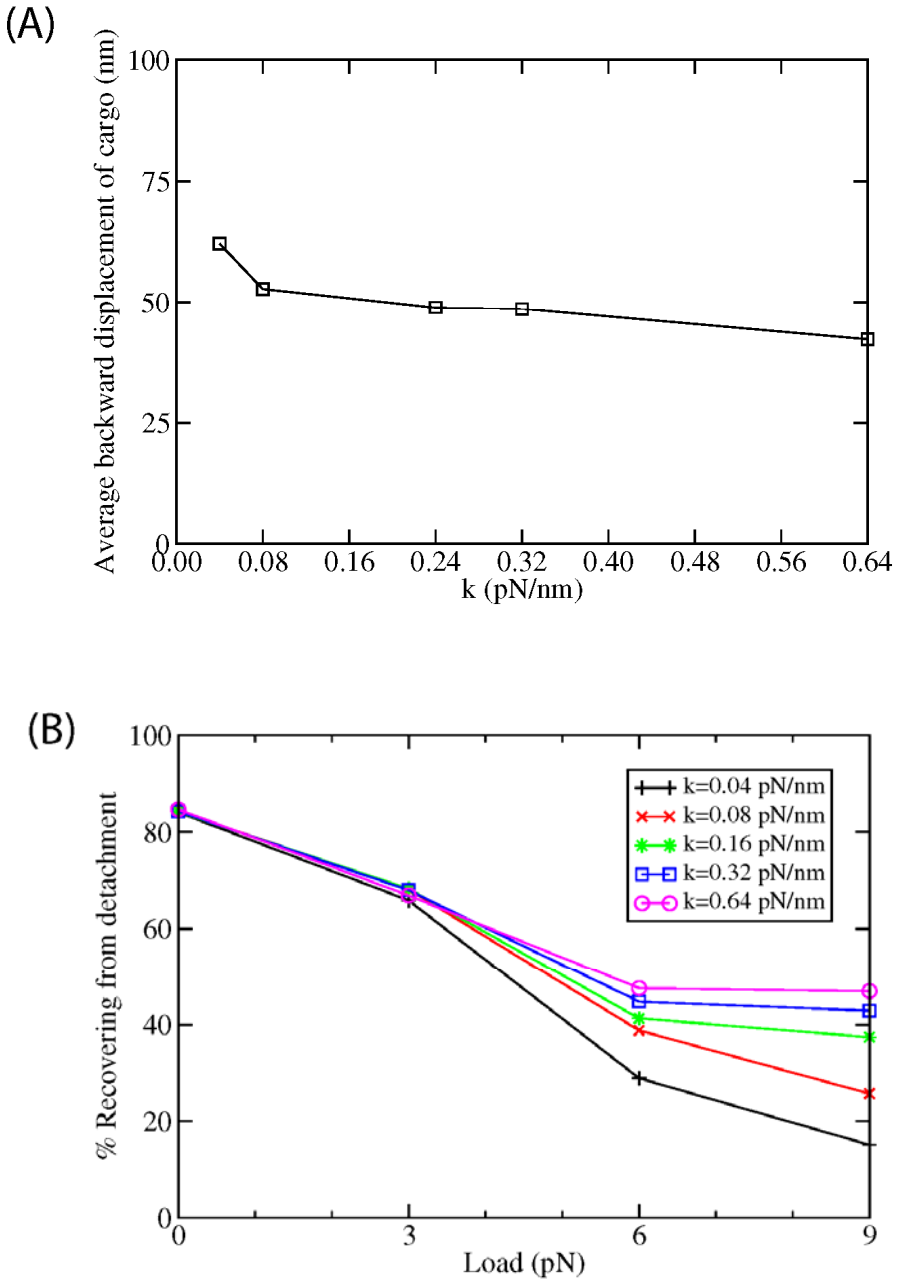

Figure S8. Backward motion of the cargo's center of mass due to motor detachment, for a cargo moved by a maximum of N=2 motors.

(A) The average backward displacement of a cargo moving under 2 pN of externally applied load, as a function of linkage stiffness obtained from Model A. Parameters chosen for MC simulation are the same as in Figure 5A (main text) except for different k values. The simulation was started with the initial condition that both motors are randomly attached to the microtubule. Monte Carlo results were obtained by averaging over 1000 samples each having a duration of 100 s. The simulation was started with the initial condition that both motors are randomly attached to the microtubule. Each run ends when either 100 seconds have passed or all the motors have detached.

(B) Successful recovery after detachment obtained from Model A. After the forward motor detaches, the cargo's center of mass moves back (with magnitude approximately that shown in A), though this also depends on applied load. Sometimes, once the detached motor reattaches and starts to move, and the cargo's center of mass starts to advance, one of the motors may again fall off before the cargo's center of mass has 'recovered' from the first detachment. The percentage of time motor doesn't fall off the microtubule, and thus recovery is successful, is shown in B. Parameters chosen for MC simulation are same as in Figure 5A except for different k values. Here, in contrast to in A), the simulation was started with initial condition that both motors are at same position on the microtubule so that they initially share the externally applied load equally. Monte Carlo results were obtained by averaging over 1000 samples each having a duration of 100 s. In contrast to in A), the simulation was started with initial condition that both motors are at same position on the microtubule so that they initially share the externally applied load equally. Each run ends when either 100 seconds have passed or all the motors have detached.

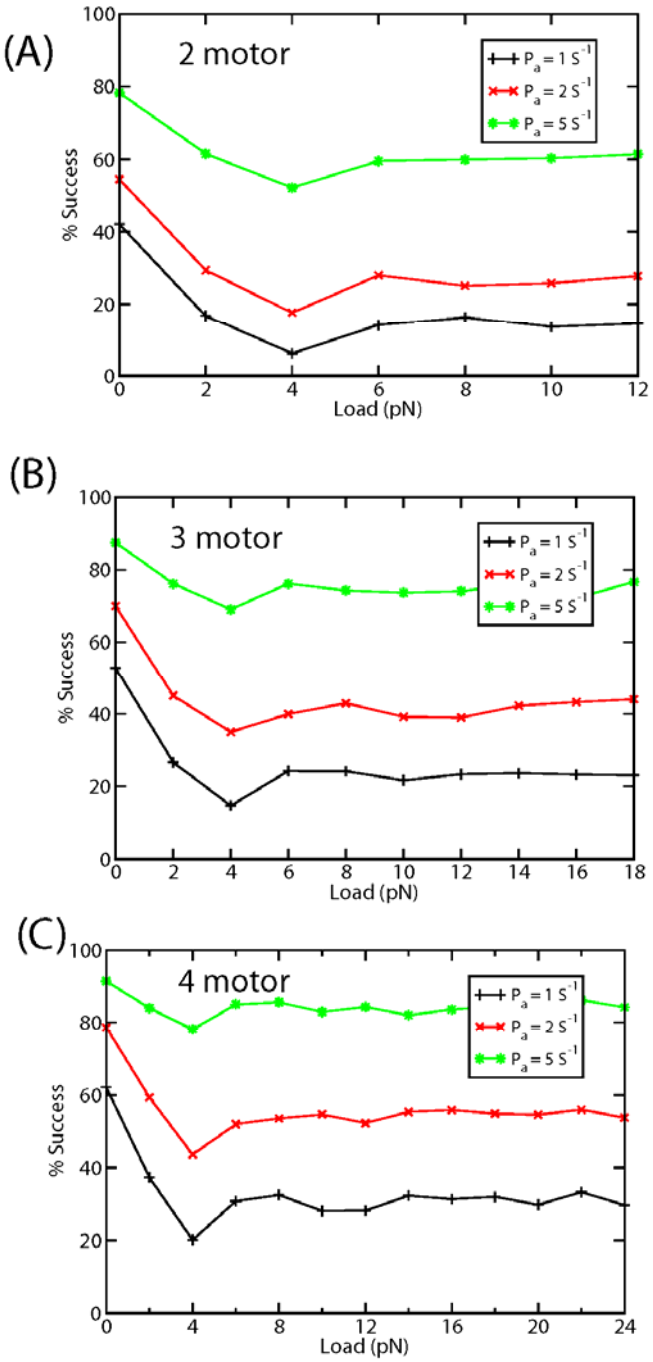

Figure S9. Percentage of cargos reaching steady state for different motor 'on rates'. Here, when the simulation is started, the initial condition is that only one motor of **(A)** N=2 **(B)** N=3 and **(C)** N=4 is attached to the microtubule. For all N values (2, 3, and 4) and on-rates (1 sec^{-1}, 2 sec^{-1}, and 5 sec^{-1}) used here, the mean number of motors engaged <n> is larger than 1, and so our initial conditions are away from the steady state number of motors attached. It is therefore possible that the cargo detaches before reaching the appropriate steady state <n> value. We investigated how likely this was to occur for

different numbers of motors on the cargo. A particular trial was judged a 'success' if the cargo stayed attached to the microtubule for the mean time to steady state (or longer). For instance, for the case of N=2 motors, the time to reach steady state for an on-rate of 1 sec^{-1} is approximately 1.25 sec (Fig. S14A, below, arrow on red curve). Thus, for (e.g.) Fig S9A (black curve) we show the percentage of cargos that stay attached for 1.25 seconds or longer. It can be seen that the particular choice of initial conditions may be important for low on-rates, because a substantial portion of the cargos fail to reach steady state, however this choice is largely irrelevant for a higher on-rate such as 5 sec^{-1} since almost all the cargos reach 'steady state'. The parameter values same as Figure 5A (main text). Monte Carlo results were obtained by averaging over 1000 samples each having a duration of 1.5 s. Simulation end when either 1.5 seconds have passed or all the motors are detached.

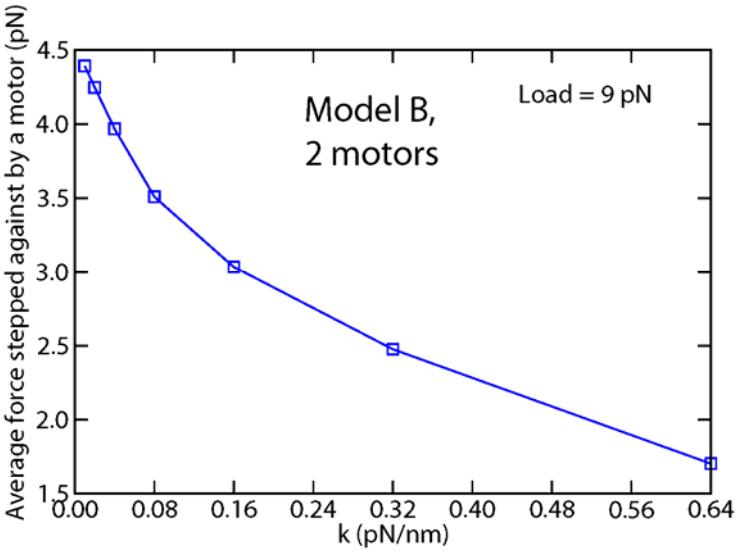

Figure S10. Strain Gating for Model B, for the case of two motors moving a cargo against an externally applied load Here, we show the average force that a motor attached to the cargo steps against in Model B, when the cargo experiences 9 pN of externally applied load, as a function of the stiffness of the linkage connecting the motors to the cargo. The initial and final conditions are identical to Figure 6A, main text, and this curve is the companion to the main-text curve for Model A (Fig. 6B, main text). The configurations were the same as for Fig. 6B, main text.

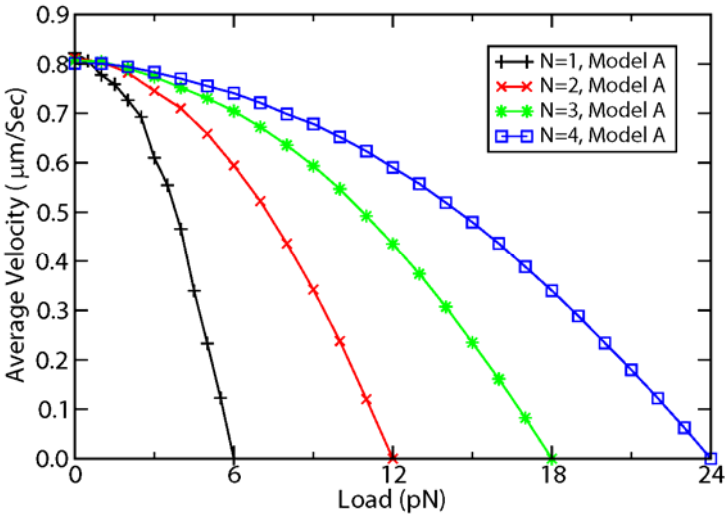

Figure S11. Force velocity curves from Model A for N=1, 2, 3 and 4 motors for linked with a linkage of stiffness k=0.04 pN/nm and without allowing detachment of motors. The parameter values are same as in Figure 4A except , B=0 μM, A=∞, P_{back}=0 s^{-1} and P_a=100000 s^{-1} to ensure that motors remain attached to microtubule all the time. The simulation was started with the initial condition that all motors are randomly attached to the microtubule. The average velocity was calculated in same manner as in Figure 4A, main text. Monte Carlo results were obtained by averaging over 100 samples each having a duration of 100s.

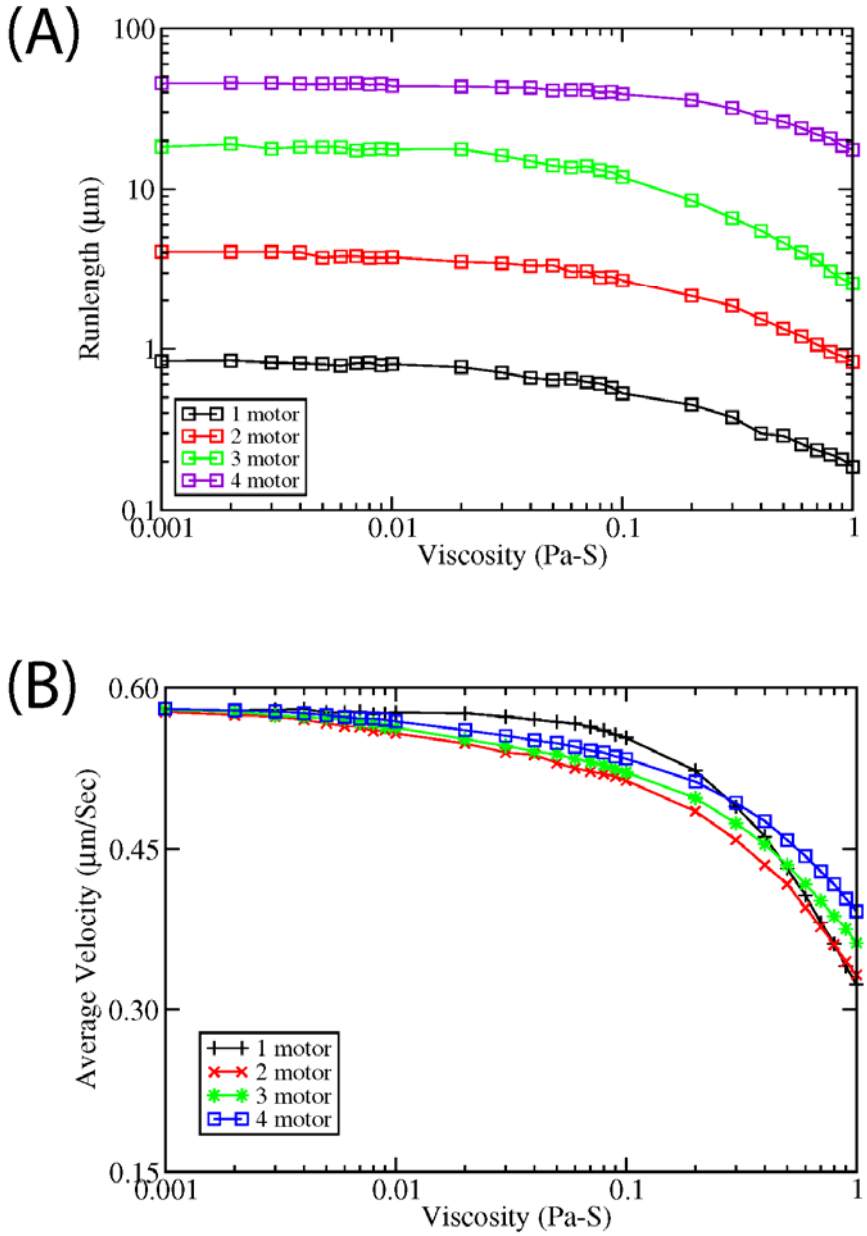

Figure S12. The effect of viscous drag on cargo transport, for 0.5 micron cargos moved by N=1 (black), 2 (red), 3 (green) and 4 (blue) motors, with a single-motor stall force of 5 pN, as predicted by Model B **(A)** Mean persistence of the cargo as function of viscosity of the medium **(B)** Average velocity of the cargo as a function of the viscosity of the medium, for motors with an unloaded velocity of ~0.6 µm/sec (chosen to match likely velocities for Drosophila lipid droplet transport). The parameter values are identical to Figure 5A (main text) except the stalling force. Similar curves for different stall forces are provided in Supp. Fig. S13.

Fig S12A. Monte Carlo results were obtained by average over 2000 samples each having a duration of 100 s (1time step=10^{-5}s). Simulation was started with the initial condition that all motors are randomly attached to the microtubule and simulation was stopped if all motors had detached

Fig S12B. Monte Carlo results were obtained by average over 2000 samples each having a duration of 100 s (1time step=10^{-5}s). The average velocity was calculated using the velocities calculated over a time window of 0.5 sec in the steady state. However for single motor average velocity was calculated over the entire run-length.

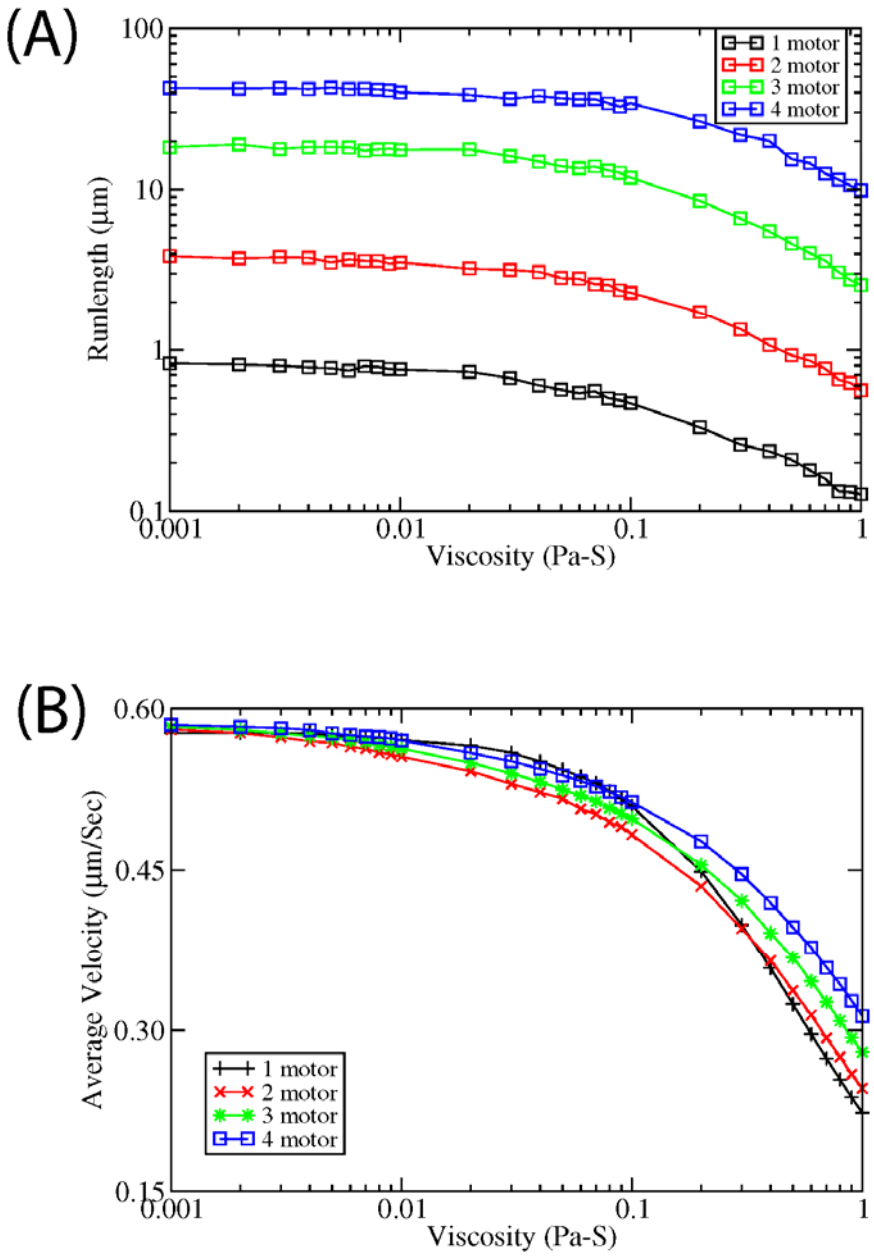

Figure S13. The effect of viscous drag on cargo transport, for cargos moved by N=1 (black), 2 (red), 3 (green) and 4 (blue) motors, with a single-motor stall force (F_0) of 2.5 pN, as predicted by Model B **(A)** Mean persistence of the cargo as function of viscosity of the medium **(B)** Average velocity of the cargo as a function of the viscosity of the medium, for motors with an unloaded velocity of ~0.6 µm/sec (chosen to match likely velocities for Drosophila lipid droplet transport). *In vivo*, it is not entirely clear what stall-force to use. We measure an apparent single-motor stall of ~2.5 pN, and thus used that to set the one-motor stall for the simulations here. However, we hypothesize that in fact the actual one-motor stall is the same *in vivo* as *in vitro* (i.e. ~5 pN), but that there is a second linkage between the cargo and the microtubule (e.g. the dynactin complex) that provides a drag of approximately 2.5 pN, so that the apparent one-motor stall we measure in vivo (that reflects the force to stall a motor, whose motion is already being opposed by this

drag) is the difference between the motor's 5 pN stall, and the 2.5 pN of velocity-independent drag, i.e 2.5 pN. Thus, the curves for a 5 pN motor are presented in the main text, Fig S12, and for a 2.5 pN stall motor here.
Number of configurations for A and B was the same as for Fig S12A and S12B, respectively.

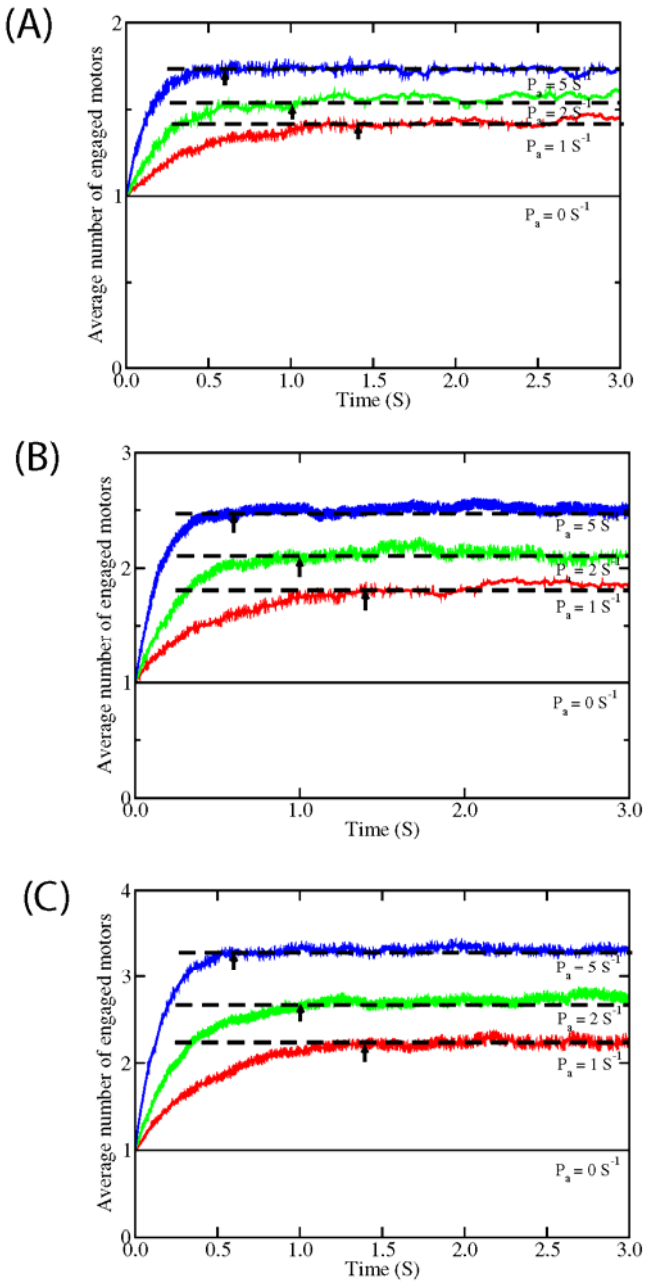

Figure S14. Average number of engaged motors with time, at different values of reattachment rates for model A for **(A)** N=2 **(B)** N=3 and **(C)** N=4 total motors on a cargo. The arrows indicate the approximate time when the system reaches the steady state behavior. The parameters used in the simulation are same as in Figure 5A (main text). Monte Carlo results were obtained by averaging over 1000 samples each having a duration of 3 s. Simulation was started with the initial condition that only one motor was attached.